Title: Emergence of an adaptive command for orienting behavior in premotor brainstem neurons of barn owls

Authors: Fanny Cazettes[1,2], Brian J. Fischer[3], Michael V. Beckert[1], Jose L. Pena[1*]

Affiliations: [1]Department of Neuroscience, Albert Einstein College of Medicine, Bronx, New York, USA

[2]Champalimaud Neuroscience Programme, Champalimaud Center for the Unknown, Lisbon, Portugal

[3]Department of Mathematics, Seattle University, Seattle, Washington, USA

Summary: The brain can be viewed as a probabilistic estimator, where sensory statistics bias judgments. Owls underestimate the direction of peripheral sound sources. This bias for central locations was proposed to reflect the increased uncertainty about eccentric direction. Understanding the neural pathway supporting this behavior provides a means to address how adaptive motor commands are implemented by neurons. Here we find that the sensory evidence about sound direction is weighted by its reliability in premotor neurons of the owl's midbrain tegmentum such that the mean firing rate approximates the head-orienting bias. We demonstrate that this coding emerges through convergence of upstream projections from a map of space. We further show that manipulating the sensory input yields changes predicted by statistical inference in both premotor responses and behavioral bias. This work demonstrates how a topographic sensory representation can be linearly read out to adjust behavioral responses by statistics of the sensory input.

INTRODUCTION

The role of internal representations of prior information and uncertainty in the synthesis of motor commands is critical for understanding how behavior adapts to sensory statistics. To address this question, we investigated the neural basis of the centrality bias of barn owls, which is a systematic underestimation of sound sources towards the center of gaze [1,2]. This centrality bias may be optimal for the owl's prey capture and can be explained by a Bayesian estimator with a prior distribution that emphasizes frontal directions [3,4]. Theoretical studies have proposed coding schemes linking behavioral biases to optimal behavior, where the amount of bias reflects the relative weights given to priors and sensory evidence depending on the reliability of the sensory input [3,5,6]. Yet, a neural circuit decoding a behavioral command that integrates the reliability of sensory evidence and prior information has not been demonstrated. This study describes how such a command may emerge in a premotor neural population that controls orienting behaviors in the sound localization system of the owl.

Most animals use interaural time difference (ITD) for inferring the horizontal direction of sound location [7,8]. In the barn owl, a map of auditory space emerges in the external nucleus of the inferior colliculus (ICx) [9], where selectivity for ITD determines the spatial tuning of auditory neurons (Figure 1). The ICx map is a distorted representation of space where the front is overrepresented [10]. It has also been shown that the frequency and spatial selectivity of ICx neurons co-vary [11], where neurons preferring frontal directions are tuned to higher frequencies than peripheral neurons (Figure 1). This direction-dependent frequency selectivity corresponds to how reliability of ITD changes across frequency and direction, estimated from the owl’s head-related transfer function [11]. Previous studies have proposed that the non-uniform spatial and

frequency selectivity across the ICx allows for the representation of prior information and ITD reliability [3,4,11].

ICx projects point-to-point to the optic tectum (OT) [12], leading to both structures having neurons with similar spatial and frequency tunings [13-14]. As a result, both ICx and OT display similar maps of auditory space, here referred to as the space-map (Figure 1). OT projects to the midbrain tegmentum (mTeg), which drives spinal-cord motoneurons that generate the head-orienting response to sound [15,16] (Figure 1). In vertebrates, the tectotegmental pathway contributes prominently to the generation of orienting movements of the eyes, head, and body [17,18]. Anatomical studies of the tectotegmental projections in the barn owl suggest that the topographic representation of space in the OT is translated into a representation of orthogonal movement coordinates in mTeg [15,16,19].

This study examined whether responses of premotor neurons in mTeg predict the owl's centrality bias, how these responses emerge, and whether they reflect the statistics of the sensory input. We found that neural responses in mTeg match the owl's behavioral bias, emerge from an effective convergence from OT to mTeg and approximate a Bayesian estimate of sound location. Furthermore, both the mTeg responses and orienting bias of behaving owls changed with manipulations of the cue reliability and sound frequency, in a manner consistent with a Bayesian estimate. Thus, we provided a mechanism for a neural system to encode a behavioral bias that approximates a combination of sensory uncertainty and prior information.

64 **RESULTS**

65 Three male and three female adult barn owls (from 3 to 5 years old) were included in the
66 electrophysiological study. We did not observe any significant difference between sexes in the
67 neural responses, therefore the data from the two groups were pooled. Behavioral experiments
68 used three different owls, two females and one male.

69 **Emergence of mTeg tuning**

70 To assess the spatial tuning of premotor neurons downstream of the midbrain space-map, we
71 conducted single-unit recording of auditory responses in mTeg using metal electrodes. Previous
72 studies have shown that microstimulation of mTeg produces head-orienting responses and eye-
73 movements [16], and that this method could be used to reliably identify this region. Although
74 these studies were successful in establishing mTeg as a region that commands orienting
75 behaviors, sound-evoked responses of these neurons were never explored. To target mTeg we
76 used the same stereotaxic [15,16] and microstimulation [16, 19, 20] guidelines reported
77 previously. For each recording site, it was verified that: 1) microstimulation at the recording site
78 elicited micro-saccades (Figure 2A,B) and 2) that microstimulation with the same current
79 intensity no longer elicited saccades after the electrode was moved a few hundred microns away
80 from the recording site.

81 Like ICx and OT neurons, mTeg neurons were tuned to ITD. For tonal stimulation, ITD curves
82 across regions displayed a similar periodic shape (Figure 3A,B). However, when broadband
83 noise was used, a notable difference was observed. Unlike neurons in ICx and OT, which display
84 ITD curves for broadband noise with a narrow larger peak flanked by smaller side peaks [21]
85 (Figure 3C), all mTeg neurons stimulated with broadband noise (n = 36; supplementary Figure

86 S1) displayed quasi-sigmodal tuning to ITD, favoring the contralateral hemifield (Figure 3D).
87 The maxima of these broadband-noise tuning curves were away from the midline on the
88 contralateral side. Although in some neurons there was a slight response decrease at eccentric
89 directions (ITD > 100 μs), this decrease was not statistically significant from the maximum
90 response across the sample (ANOVA, p (F>0.4) = 0.92). Therefore, ITD-tuning curves in
91 response to broadband-noise in mTeg can be considered largely monotonic, with responses
92 increasing across the midline, and reaching a plateau at eccentric locations in contralateral space.

93 We tested whether the transformation from a peaked ITD tuning to monotonic curves was
94 consistent with a convergent projection from OT to mTeg, as proposed for the midbrain network
95 guiding eye saccades [22]. If mTeg neurons received convergent input from OT, their responses
96 should reflect the varying ITD and frequency selectivity of OT neurons across the space-map
97 [11,14] (Figure 1). To verify this hypothesis, we tested two specific predictions for the
98 convergence from OT to mTeg on auditory responses: 1) because frequency tuning varies across
99 the space-map [11,14], a downstream neuron receiving convergent input from OT should have
100 broader frequency tuning; and 2) because ITD tuning covaries with preferred frequency in ICx
101 and OT [11,14], stimulation with tones will drive activity in only a subset of the cells exciting
102 each mTeg neuron. Thus varying frequencies should alter the mTeg ITD tuning curve shape in a
103 manner consistent with how frequency and ITD tuning change in ICx and OT.

104 To test the first prediction, we measured the half-width of frequency tuning curves in ICx, OT,
105 and mTeg neurons. Frequency tuning curves of mTeg neurons were significantly broader than
106 ICx and OT (Figure 3E,F, mean ± s.d difference in frequency bandwidth: 2.4 kHz ± 0.3 kHz, $p <$
107 10^{-11}, Wilcoxon rank-sum test). This result is consistent with a convergence from OT into mTeg.

To test the second prediction, we measured ITD tuning in mTeg for tonal stimulation, within the range of frequencies that elicited significant responses. As reported above, the ITD tuning curves of mTeg neurons measured with tonal stimulation were sinusoidal functions with the period determined by the stimulating frequency (Figure 3B,G). Remarkably, unlike in ICx and OT, where neurons prefer the same ITD at all frequencies they respond to, i.e., they display a characteristic delay [21], mTeg neurons' preferred ITD varied with frequency (Figure 3G,H). For each cell, the peak ITD shifted towards 0 μs when the stimulus frequency increased (Figure 3H, right, $r^2 = 0.85$, intercept=250 μs, slope= -0.042 μs/Hz, $p<0.001$). Moreover, the change in preferred ITD with frequency of mTeg neurons was strongly correlated with the change in frequency and ITD tuning in the space-map [11] ($r^2 = 0.75$, intercept=284 μs, slope= -0.045 μs/Hz, $p<10^{-55}$), where frontal neurons, tuned to ITDs near zero, prefer higher frequencies than peripheral neurons tuned to large ITDs [11,14]. These results provide physiological evidence of a convergence from OT into mTeg.

Weighted convergence from space-map to mTeg

It was shown above that mTeg tuning to ITD and frequency are consistent with a convergence that takes place between the space-map in OT and mTeg. We next asked whether the mTeg responses can be explained by a weighted linear convergence from space-map neurons, a processing scheme that has been proposed for the emergence of motor commands [22,23]. For this, a bank of ITD tuning curves of a population of OT neurons was modeled following criteria from published tuning properties of space-map neurons. Specifically, cells tuned to frontal ITDs are overrepresented, prefer higher frequencies, and therefore display narrower ITD tuning [11, 14] (Figure 4A). This modeled OT population was the same used previously for Bayesian decoding analyses [3,10,24], as well as in the next section of the present study. Modeled OT

131 tuning curves were then weighted, i.e., rescaled (Figure 4B,C), and summed (Figure 4D) to
132 simulate the weighted convergence. To estimate the weights at each frequency/ITD channel
133 converging onto mTeg cells, we used linear decomposition by Fourier analysis of ITD tuning
134 curves for broadband noise of mTeg neurons. It has been shown that this method can be used to
135 efficiently assess the neurons' frequency responsiveness [25] (Figure 4B; see supplementary
136 Figure S2 for similar analysis using random weights). Here, a higher power at a specific
137 frequency in the Fourier decomposition of the broadband-noise ITD response of an mTeg neuron
138 corresponds to a higher weight applied to the projecting OT neurons corresponding to that
139 frequency (Figure 4A-C). The weighted OT ITD-tuning curves were then summed and the output
140 was compared to the actual ITD tuning of mTeg neurons on a cell-by-cell basis (Figure 4D). We
141 observed good correlations between modeled and measured mTeg ITD-tuning curves (Figure 4E,
142 pairwise linear correlation, $p<0.05$ for 34 out of 36 neurons, median variance explained = 70%),
143 indicating that ITD tuning of mTeg neurons to broadband sound could be predicted from the
144 weighted convergence of the space-map population. These results indicate that mTeg responses
145 are consistent with a weighted linear convergence from the midbrain space map, a plausible
146 mechanism in neural processing [22,23].

147 **Emergence of an adaptive orientation estimate in mTeg**

148 We next examined whether mTeg responses approached an optimal motor command by
149 integrating ITD information and the reliability of this cue in the sensory input. In neural theory
150 of probabilistic inference, a Bayesian estimate of a specific sensory feature results from the
151 integration of sensory input and prior information about this feature. This integration is done
152 while weighting the sensory input by its reliability. As a result, if sensory information is
153 degraded (i.e., unreliable), a Bayesian estimate will increasingly be biased toward the prior

154 information. To manipulate the reliability of the ITD cue in a quantitative manner, the similarity
155 of the sound at the left and right ears was varied by adding uncorrelated noise (referred to as
156 binaural correlation; BC). Lowering BC increases the sensory noise. In space-map neurons this
157 decreases the amplitude and broadens the ITD-tuning curves [26,27].

158 We investigated: 1) if mTeg responses can be explained by a Bayesian estimator, and 2) if these
159 responses predicted behavior when the reliability of the ITD cue changed. To answer the first
160 question, we read out sound source direction from the modeled population of OT neurons
161 described above as BC changed, using a Bayesian decoder (maximum a posteriori (MAP); see
162 supplementary Figure S3 for similar estimates using the mean of the posterior). Then, we
163 examined whether mTeg responses were consistent with the output of the MAP decoder when
164 BC changed. To answer the second question, we examined if mTeg responses predicted behavior
165 as BC levels changed.

166 The barn owl's sound localization accuracy can be predicted by Bayesian inference with a prior
167 for frontal space, i.e. frontal sound locations are considered more likely [3, 4]. Consistent with
168 the general properties of Bayesian inference explained above, the MAP estimate of sound source
169 direction applied to the modeled OT population showed an increasing bias toward the center of
170 gaze as BC decreased [27] (Figure 5A).

171 Interestingly, mTeg responses also varied with BC in a manner consistent with the MAP estimate
172 of sound direction (Figure 5A-D). Specifically, the mean normalized firing rate of mTeg neurons
173 in the sample was highly correlated with the Bayesian estimate at each BC (Figure 5A,B, mean
174 r^2=0.75, $p<10^{-22}$). Additionally, the change in the standard deviation of the mean mTeg
175 population response also correlated well with the standard deviation of the MAP estimate (Fig.
176 5C,D, r^2=0.84, p=0.01). Previous work has also demonstrated that the bias of the MAP estimate

177 across BCs does not change significantly until BC decreases below 0.5 [3,26,27]. To further
178 confirm the correspondence between mTeg responses and the MAP estimate, we examined
179 whether this feature was also present in mTeg population responses. Towards this end, we
180 examined how much mTeg responses for a given ITD changed as BC was decreased. As
181 observed in the MAP estimate, mTeg responses for a given ITD did not change significantly
182 when BC remained above 0.5 (Figure 5B,D blue, ANOVA, p(F=0.03)=0.97), whereas responses
183 when BC was below 0.5 were significantly different from when BC was equal to 1 (Figure 5B,D
184 green Tukey post-hoc test, $p<0.05$). Altogether, these results show that the mTeg response
185 changes consistently with the MAP estimate.

186 In addition to investigating the correspondence between mTeg responses and MAP estimate, we
187 examined whether mTeg responses and the sound localizing behavior were matched across BC.
188 For this, we relied on data previously reported, showing that the changes in the owl's behavioral
189 bias with varying BC (Figure 5E reported in [26]) were highly correlated with the MAP estimate
190 (mean r^2 for the four stimulus directions=0.95, $p<10^{-3}$; see Figure 6C in [27]). Here, to compare
191 the mTeg responses with the owl's localization data, we plotted mTeg responses as a function of
192 BC for the same four ITDs used in the published behavioral experiments. These mTeg responses
193 were well correlated with behavior (Figure 5F, mean r^2 for the four stimulus directions = 0.84,
194 p=0.017).

195 Finally, we examined whether the bias predicted by the MAP estimate, the bias in mTeg
196 responses, and the owl's behavioral bias matched as BC changed. To compare the bias in MAP
197 estimate, mTeg responses, and behavior, we computed the mean difference between responses at
198 BC= 1 and at lower BCs (Figure 5G,H,I). The MAP estimate predicted an increased bias at lower

199 BCs (Figure 5G). The same trend was observed in both the mTeg population response (Figure
200 5H) and in the orienting behavior of the owl (Figure 5I).

201 Overall, the correlations between mTeg neural responses, Bayesian (MAP) decoder predictions,
202 and behavior across BCs support the hypothesis that mean mTeg responses approximate an
203 estimate of sound direction that changes adaptively when the sensory input is degraded.

204 **Testing the network architecture by manipulating the owl's behavioral bias**

205 In light of the physiological and theoretical evidence of an adaptive behavioral command
206 emerging in mTeg, we set out to test if the weighted convergence across the space-map by mTeg
207 neurons was predicted by the MAP estimate and subsequently consistent with the owl's orienting
208 behavior. To this end, we aimed to selectively manipulate the activity in different parts of the
209 space-map and verify whether these manipulations yielded consistent changes in the MAP
210 estimate and the owl's behavior. To achieve this goal, we relied on previously published
211 evidence showing that frontal and peripheral space-map neurons are tuned to high and low
212 frequencies, respectively [11,14]. Therefore, stimulation with a sound containing only high
213 frequencies should enhance the response of frontal neurons relative to peripheral neurons, with
214 the converse occuring for stimulation with low frequency (Figure 6A). Hence, when the
215 frequency band of the stimulus is changed, the differential activation of neurons across the
216 space-map should be reflected in the predictions of the MAP estimate, the mTeg responses, and
217 ultimately the owl's behavior. To test this hypothesis, we first examined predictions of the MAP
218 estimate when the modeled population of space-map neurons was stimulated with high and low
219 band-pass noises and tested these predictions on mTeg neurons. Then, we asked if the owl's
220 sound localizing behavior was consistent with predictions of the weighted convergence.

221 The MAP estimate predicted that at peripheral locations, mTeg responses to high-frequency
222 sounds should be lower than mTeg responses to low-frequency sounds (Figure 6B, p=0.021,
223 Wilcoxon rank-sum test). Thus, if mTeg responses approximate a MAP estimate, the firing rate
224 of mTeg neurons should be more strongly driven by low frequencies within peripheral ITDs than
225 by high frequencies. Remarkably, mTeg responses were consistent with the MAP estimate
226 predictions, displaying significantly different responses for the two types of stimulation, where
227 mTeg neurons displayed lower firing rate at peripheral ITDs for high than low frequencies
228 (Figure 6D, ANCOVA, p(F=9.93) $<10^{-3}$). Similar to the MAP estimate, mTeg responses to high
229 frequency stimuli were less monotonic than at low frequencies, displaying shallow peaks and
230 troughs (Figure 6B,D, peaks of the MAP estimates at -190 μs and +160 μs; peaks of the mTeg at
231 -190 μs and +150 μs). These peaks and troughs for high frequency stimulation are expected from
232 the phase-ambiguous ITD information of high frequency stimuli within the ITD range tested (see
233 example in Figure 3G, purple curves). However, this is not inconsistent with the prediction of the
234 weighted-convergence network architecture that at larger ITDs the firing of mTeg neurons is
235 higher. Thus, the ITD tuning of mTeg neurons stimulated with high and low band-pass noises
236 was consistent with the predictions of the MAP estimate.

237 We next tested whether the changes observed at different frequencies predicted a change in
238 behavioral performance. Interestingly, the MAP estimate predicted different behavioral biases at
239 high and low frequency (Figure 6C, low frequency average bias of 13.2 deg; high frequency
240 average bias of 27.6 deg). This prediction was matched by mTeg responses (Figure 6E, low
241 frequency average bias of 14.3 deg; high frequency average bias of 31.4 deg).

242 We then tested whether the owl's behavioral bias was indeed consistent with the MAP estimate
243 and the responses of mTeg neurons. For this we measured non-reinforced head-turns triggered by

high and low-frequency band-pass as well as broadband sounds in behaving barn owls. Training was limited to standing on a perch at the center of a speaker array; in this way we avoided potential influences of over-training [28] (Figure 6F). The owl's natural tendency to orient the head toward sounds was tracked with high-speed infrared cameras (Figure 6G). Head-saccades were measured from any initial head angle to avoid positional biases. To control for the confound between centrality bias and unwillingness of the barn owls to turn the head for sounds close to the center of gaze, sound sources within 10 degrees or less from the center of gaze at the time of sound presentation were not included in the analysis. We then estimated the average bias as the mean difference from the actual sound source direction. Using this paradigm, owls underestimated peripheral directions for broadband noise (the average bias over all eccentric directions was 21 deg), as reported in previous studies using owls trained to fixate at the front and motivated to respond through reward [1,2]. Remarkably, owls showed significantly stronger underestimation when localizing high frequency sounds than low frequency sounds (Figure 6H left, $p<10^{-4}$, permutation test; average bias at high frequency: 27 deg; average bias at low frequency: 13 deg, see supplementary Figure S4 for the performance of each owl). Thus, the amount of behavioral bias could be adjusted upward and downward by targeted manipulations of the sensory input that elicited corresponding changes in mTeg activity.

In summary, the correlation between the MAP predictions, mTeg neural responses, and behavioral bias observed during frequency manipulations of the auditory signal indicates, independently from the BC manipulations, that mTeg responses could account for the behavioral bias by integrating across the space-map population, approximating an adaptive command for the owl’s orienting behavior.

DISCUSSION

This work explained how the midbrain map of auditory space is read out by downstream neurons to synthesize a command of orienting behavior that captures sensory uncertainty. It has previously been shown that the selectivity of space-map neurons reflects cue reliability [11] and proposed that this property may be a crucial parameter for guiding an adaptive behavioral bias [27]. However, how precisely changes in space-map neurons' selectivity are translated into an adaptive behavior was left unanswered. The present study shows how the space-map population may be read-out by downstream neurons to guide behavior in situations of uncertainty. Here, we demonstrated that this processing is consistent with a weighted convergence from the OT to mTeg, generating a conversion from a map representation to a rate-code, driving orienting behavior weighted by sensory reliability. Based on these mechanistic findings, predictions were made about how the adaptive behavioral bias would change by controlling stimulus frequency. These predictions were confirmed with behavioral experiments, allowing further demonstration of the network architecture by manipulations at the encoding level. Therefore, we show here how sensory statistics can be biologically decoded into a signal controlling head saccade. This is a major conceptual advance over previous work.

Sensory-motor integration

Critical findings of this study are the evidence of convergence from OT onto mTeg and the effect this convergence has on the ITD tuning in mTeg. Convergence from the space-map is supported by the broader frequency tuning of mTeg neurons and their frequency-dependent ITD tuning, which matches the ITD-dependent frequency tuning in ICx and OT previously reported [11,14]. The remarkable consistency of how best ITD changes with frequency in mTeg with how best frequency changes with ITD in ICx [11] and OT [14] indicates that convergent projections of

290 neurons from the space-map explains the tuning in mTeg. Thus, mTeg neurons lacked the classic
291 characteristic-delay described for neurons of the inferior colliculus [21]. This is also consistent
292 with the dramatically different response to ITD with broadband stimulation in mTeg, compared
293 to ICx and OT, where mTeg responses appear quasi-sigmoidal while ICx and OT responses
294 display peaked and largely symmetric rate-ITD curves around a prominent preferred ITD.

295 A fundamental question in sensorimotor integration is the neural code controlling movement
296 [23,29-31]. Previous studies have reported correlations between the firing rate of sensorimotor
297 neurons and the kinematics of movements [29]. Here we propose that the premotor neurons in
298 mTeg encode direction in the population average firing rate, which, through weighted
299 convergence, captures the statistics represented in the upstream space-map. This is consistent
300 with the idea that mTeg neurons control muscle synergy rather than single muscles
301 independently [19,30,31], which has been proposed for explaining why correlations between
302 neuronal responses and movement properties are commonly observed [29].

303 The dorsal and medial tegmental areas are composed of multiple nuclei that receive direct
304 projections from the OT. Microstimulating these areas yields head-saccades in different
305 directions [16]. Therefore, populations of mTeg neurons in distinct nuclei are likely to have
306 different tuning properties. Here, we focused on the horizontal coordinate of sound direction,
307 which in barn owls is specifically linked to the coding of ITD [32]. Hence, we targeted mTeg
308 neurons with clear tuning to ITD throughout mTeg. While the purpose of this study was to
309 develop a normative model of the emergence of an adaptive motor command for head
310 lateralization and elucidate the underlying functional network, we did not attempt to completely
311 explain the anatomical pathway supporting head-orienting responses. Further experiments are

312 needed to explore the heterogeneous and likely complex properties of mTeg neurons that
313 participate in guiding eye and head movements in different directions.

314 **Implementation of an adaptive behavior**

315 In general, behavioral errors are composed of systematic errors (biases) and precision errors
316 (variance). A minority of studies have focused on behavioral biases to understand the underlying
317 neural code [6,33-36]. Yet, focusing on the bias itself can provide information about the strategy
318 the brain uses to produce adaptive behavior. Although both bias and variance contribute to the
319 magnitude of errors, they provide different insights into how errors may occur in judgments.
320 While the variance may reflect the level of confidence in either the evidence or the estimate, the
321 systematic nature of the bias and its direction can be interpreted as the manifestation of a prior
322 [3,5,27,34] or a cost function [37] that constrains the judgment. Understanding the neural
323 response properties that emerge from the underlying circuitry in the owl's sound localization
324 pathway made it possible to manipulate the behavioral bias using specific sensory stimuli. These
325 findings may also be testable in other species where auditory biases have been observed,
326 including humans [3,38-40].
327 The goal of this study was going beyond presenting the Bayesian model as a normative approach
328 of how evidence about sound direction can be weighted by cue reliability, but to demonstrate the
329 network implementing the neural command guiding a behavioral response weighted by the
330 uncertainty in sensory information. The normative model does not recapitulate exactly the neural
331 and behavioral variability. However, it helps in interpreting the experimental results from the
332 Bayesian approach perspective, i.e. that the adaptive behavioral bias reflects the statistics of the
333 sensory input. The MAP estimate and mTeg responses were highly correlated in shape and
334 changed consistently across independent conditions (sound frequency and BC). However, the

335 MAP estimate did not perfectly match the mTeg responses. Despite a correspondence in shape
336 and pattern of change across BCs, we observed that at negative (ipsilateral) ITDs, the mTeg
337 responses appeared more monotonic than the MAP estimate for higher BCs. For both
338 hemispheres neural responses were maximal for sound directions within the contralateral
339 hemifields. Yet, mTeg receives inputs from the left and right OTs [15]. Thus, although the
340 orienting behavior is presumably controlled by activity from both sides of the midbrain
341 tegmentum [16,19], it is likely that the stronger firing rate elicited by sounds on the contralateral
342 side, which matches better to the MAP estimate, have a stronger influence on guiding orienting
343 responses [16,19]. In addition, although variability of the MAP estimate and mTeg responses
344 changed in the same direction with BC, the absolute numbers are different, with the change in
345 variability from BC = 1 to BC = 0.1 being an order of magnitude larger for the MAP estimate.
346 Variations of the MAP estimate from one trial to another reflect the population response, where
347 neural variability is correlated, while mTeg standard deviation reflects changes in the response of
348 single neurons. Thus, the across-trial variability of the MAP is influenced by correlated noise in
349 the modeled space-map population, while this correlated noise is not captured in the variability
350 observed when averaging across individual mTeg responses, possibly leading to the difference in
351 absolute levels predicted by the model and observed in averages of mTeg responses recorded
352 separately.

353 Explaining biased behavior with Bayesian theory has implications for understanding sensory
354 perception [3,5,41]. Bayesian inference shows how combining prior and sensory information
355 predicts optimal perception of ambiguous sensory inputs [41-46]. However, theoretically optimal
356 methods are but metaphors for how the brain actually decodes information, and the fact that
357 mTeg responses approximate the Bayesian estimate is not trivial. Although both the specific

358 Bayesian estimate tested in this study and the weighted convergence act as linear decoders, they
359 could not be explained by any arbitrary linear convergence network. For example, a point-to-
360 point projection from OT to mTeg would produce a similar population code for direction to those
361 seen in ICx and OT, rather than a rate code reflecting movement direction. Additionally, a
362 random linear convergence from OT to mTeg did not necessarily predict the mTeg response and
363 approximate a Bayesian decoder (see supplementary Figure S2). Rather, a specific integration
364 across frequency and ITD was required for the convergence from OT to mTeg to approximate
365 the Bayesian direction estimate. Thus a precise, yet simple and biologically plausible mechanism
366 of weighted convergence explains how the neural code for sound localization can be translated
367 into an adaptive behavioral command.

368

369 **MATERIALS AND METHODS**

370 **Electrophysiology**

371 *Surgical procedure:* Surgery was performed as described previously [47]. Briefly, adult barn
372 owls (3 females and 3 male) were anesthetized with intramuscular injections of ketamine
373 hydrochloride (20 mg/kg; Ketaset, intramuscular) and xylazine (4 mg/kg; Anased,
374 intramuscular). Prophylactic antibiotics (ampicillin; 20 mg/kg, intramuscular) and lactated
375 Ringer's solution (10 ml, subcutaneous) were injected at the beginning of each session. An
376 analgesic (Carprofen; 3mg/kg, Rimadyl, intramuscular) was administered at the end of each
377 session to prevent inflammation and pain. These procedures complied with National Institutes of
378 Health and guidelines of the Albert Einstein College of Medicine's Institute of Animal Studies.

379 Recording from awake animals was impractical in these experiments as electrophysiology
380 required serial electrode penetrations, head restraint, and long recording sessions (up to 10
381 hours). To control for varying levels of anesthesia, records of the time of each recording relative
382 to anesthetic administration were rigorously maintained. Experiments were interrupted when
383 latencies or response thresholds changed. Regardless, the effect of anesthesia in the midbrain has
384 been shown to be less pronounced than in the forebrain [48,49] and therefore lessens concerns
385 about changes in neural response under anesthesia.

386 *Extracellular recordings of ICx, OT and mTeg neurons:* Single-unit responses were recorded
387 using 1MΩ tungsten electrodes (A-M Systems). Tucker Davis Technologies (TDT) System 3 and
388 custom written Matlab software (Mathworks) were used to record neural data. ICx and OT were
389 located stereotaxically and confirmed by the characteristic responses to ITD and interaural level
390 difference and firing properties [47]. The mTeg was also located stereotaxically [15,16] but
391 recording from this structure was further verified with microstimulation (see below).

392 *Microstimulation:* Recordings in mTeg were confirmed with microstimulation. At the end of
393 each recording, microstimulation at the recording site was conducted to verify that eye
394 movements were elicited and that the same electrical stimulus was no longer able to elicit eye
395 movements when the electrode was moved a few hundred micrometers away from the recording
396 site. A programmable digital stimulator (WPI, DS8000) was used to deliver trains of current
397 pulses (5ms pulse width, 200Hz, 80ms duration) through the recording electrode, varying the
398 current amplitude from 50 to 150 μA with inter-stimulus intervals larger than 15 seconds (as
399 described in [20]). In most experiments, 130 μA or less was enough to induce unequivocal eye
400 movements (see Figure 2 for example).

401 **Sound stimulation**

402 All experiments were performed inside a double-walled sound-attenuating chamber. Custom-
403 made earphones consisting of a calibrated speaker (Knowles model 1914) and a microphone
404 (Knowles model EK-23024) were inserted in the owl's ear canal [47]. Auditory stimuli delivered
405 through the earphones consisted of 100 to 150 ms signals with a 5 ms rise-fall time at 10-20 dB
406 above threshold. For each ICx, OT, and mTeg neuron, we first measured the ITD and rate-level
407 response with broadband noise (0.5 – 10 kHz). ITD was initially varied from ±300 μs with 30 μs
408 steps over 5-10 trials for ICx and OT and 20 trials for mTeg. Sound level varied from 0 dB SPL
409 to 70 dB SPL in 5-dB steps. Frequency tuning was measured with tones ranging from 500 Hz to
410 8000 Hz varied in 200 to 500 Hz steps over 20 trials. Neural responses to ITD in mTeg were also
411 recorded at various frequencies (from 1 to 6 kHz, 1 kHz steps, same ITD protocol as broadband).
412 Stimuli within all tested ranges were randomized during data collection.

413 To manipulate the binaural correlation, three random noise signals (N1, N2, and N3) were
414 generated. N1 was delivered to one ear and its copy with a time shift, to produce an ITD, was

415 delivered to the other ear. N2 and N3 were added to the N1 in the left and right ear respectively.
416 These additional noise signals reduced the correlation between the signals in the two ears,
417 depending on the relative amplitudes of the uncorrelated and correlated noises. Binaural
418 correlation was calculated from $BC = 1/(1 + k^2)$, where k is the ratio between the root-mean-
419 square amplitudes of the uncorrelated and correlated noises [26]. On a subset of ICx neurons
420 (n=46) and on all recorded mTeg neurons, we obtained ITD curves (+/- 300 µs; 30 µs steps; 20
421 repetitions) using noise bursts at different BCs (from 0 to 1, in 0.2 steps).

422 Finally, for all mTeg neurons we measured ITD curves (+/- 300 µs; 30 µs steps; 20 repetitions)
423 with low (500-3500 Hz) and high (4500-7500 Hz) frequency band-pass sounds as well as
424 broadband noise (500-9000 Hz).

425 **Behavior**

426 *Remote eye tracking*: Eye movements triggered by microstimulation in mTeg were measured
427 with high-speed video imaging using a commercially available eye tracking system (EyeLink
428 1000) that detected the pupil and the position of the corneal reflection. Eyelids were opened
429 momentarily to conduct the test after each recording using a custom made retractor. This
430 procedure and the anesthesia did not prevent blinking of the nictitating membrane allowing for
431 natural protection of the eyes from drying.

432 *Head-orienting behavior:* Head-orienting behavior to sound was measured for three hand-raised
433 barn owls trained only to stand on a perch at the center of a speaker array. The speaker array
434 consisted of an azimuthal linear array of 21 speakers, a subset of a hemispherical array of
435 speakers constructed inside a sound-attenuating chamber [47,11]. The linear array spanned 100
436 degrees to the left and right of the midline, with 10 degrees separation between speakers. Each
437 speaker was calibrated in place using a microphone mounted on a pan-tilt robot located at the

array center. Head saccades were recorded with a pair of high-speed infrared cameras (Fastec Imaging, 100 frames per sec) mounted in the corners of the room. Head saccades were then tracked using custom designed image-analysis code (Xcitec, Proanalyst) from images calibrated in 3-D using a grid located at the same position of the owl's head. Owls were presented with the same noise bursts used to measure neural responses (100 ms long, 5 ms rise-fall time, high and low frequency band-pass sounds, and broadband-noise) but through this free-field array. The setup allowed us to measure head saccades from any starting head position, which made it possible to rule out positional biases. To account for the position of the animal in the field of view of the cameras, the owl's perch was designed such that it only allowed the bird a single stance. However, owls did not always look straight ahead when the stimulus was presented; therefore, the measured angles of head turn were transformed into a head-centered coordinate system. Owls were unrewarded in this task to avoid biases introduced by training. As a consequence, they only performed a few orienting-responses per experimental session [28], requiring long periods of rest and repeated sessions over more than two years to collect the data. For each sound presentation, the frequency band (0.5-3.5 kHz, 4.5-7.5 kHz or 0.5-9 kHz) and location (±100 deg, 10 deg separation) of the source were randomized by the software. The experimenter initiated a trial when the owl was standing upright and its beak (the tracking reference, see Figure 6G) was in the field of view of both cameras. The experimenter remained blind to the properties of the sound.

Data analysis

Electrophysiological data: For each stimulus parameter, a rate curve was computed by averaging the firing rate during sound stimulation over trials. The spontaneous firing rate, obtained when no sound stimulation was presented, was subtracted from the response to the stimulus. Best ITDs

were defined as the center of the range that elicited 50% of the maximum response of each tuning-curve. To assess the relative broadness of the frequency tuning we calculated the areas under the normalized frequency tuning curves. To find the peak of ITD-tuning curves of mTeg neurons to tonal stimulation we first fitted the curves with a cosine function. We then defined the ITD corresponding to the closest maximum from 0 μs as the peak [11]. The changes of ITD tuning with BC were consistent in both hemispheres (maximal changes for sound directions within the contralateral hemifields). Thus, analyses of the mean mTeg response were performed on the combined data, normalized to contralateral and ipsilateral side leading.

ITD increases with eccentricity [32]: small values of ITD (~0 μs) are associated with frontal directions and larger values of ITD (~200 μs) are associated with the periphery. Thus, we converted ITD to azimuth [32] to measure the bias predicted by the mTeg response to ITD.

Behavioral data: Head orientation and angular velocity were computed offline using image-analysis software (Xcitec, Proanalyst). Individuals analyzing the data remained blind to the location of the sound source until the end. Subsets of the data were analyzed independently by different persons to confirm the analysis was consistent across individuals. Trials where owls moved during the presentation of the stimulus or where the beak disappeared from the field of view of the cameras were discarded. We measured saccade latencies as the time from the onset of each presentation of a stimulus to the first video frame where the owl's head started rotating. Median latency varied across animals (owl L=240 ms; owl F=520 ms; owl P=210 ms). These values are higher than previous reports [1,18,50]. However, most previous studies were conducted with trained owls that were rewarded if the saccade was correct. For each owl, there was no significant difference between the latencies across stimulus conditions. Saccades whose latency was greater than 1 sec were discarded. Based on angular velocity, head movements

484 during a saccade were classified as rotation, translation, or fixation [51]. Consistent with the
485 literature, we only included head rotations with an angular velocity greater than 50 deg.sec^{-1}
486 [18,50,51]. When translational movements were included in the analysis the results remained
487 consistent, albeit more variable. The criteria for classifying movements as saccades became
488 unreliable when the sound source was close to the front [1,50], therefore only head-turns evoked
489 by sources located 10 degrees away from the initial head angle were included in the analysis.

490 **Modeling**

491 *Heterogeneous population of neurons in the space-maps:* We modeled a space-map population
492 of 500 neurons. To incorporate the overrepresentation of frontal space into the modeled
493 population, the density of preferred direction X was drawn from a Laplace prior:

494 $$p(X) \propto \exp\left(-\frac{|X|}{b}\right),$$

495 where the scale parameter is b=25 [3,10]. First, broadband noise signals between 0.2 and 12 kHz
496 were passed through a gammatone filter-bank with center frequencies ranging from 0.25 kHz to
497 8 kHz in 0.25 kHz steps. The time constants of the filters were specific to the owl and estimated
498 from Koppl [52] to model cochlear filters, as described in [24]. The outputs were cross-
499 correlated and transformed by an exponential input-output function to produce a set of
500 frequency-dependent ITD curves (from 0.5 to 8 kHz). The input to ICx was modeled as a
501 weighted sum of the frequency-dependent ITD curves. The weights were direction-dependent to
502 model the direction-dependent frequency tuning in ICx [11]. The weights for each neuron have a
503 Gaussian shape with a center and width selected to match the observed frequency tuning at the
504 preferred direction of the neuron. The weighted sum of the frequency-dependent ITD curves was
505 passed through an exponential nonlinearity to produce the firing rates of Poisson neurons that

506 modeled ICx responses. The responses in OT, which receive point-to-point projections from ICx
507 [12], are influenced by feedback inhibition that serves to select the dominant stimulus when
508 multiple peaks of activity are present in the map [53,54]. To model OT neurons, we used a
509 simplified version of the model of Mysore and Knudsen (2012, 2014) by multiplying the ICx
510 activity pattern by a rectangular window function to select the dominant peak. The window takes
511 a value of one on an interval that is 28 degrees wide centered at the location of the peak in a
512 smoothed version of the ICx activity pattern. The decoding analyses were applied to the
513 windowed response pattern representing the population activity of the OT.

514 Assuming a linear transformation between OT and mTeg, the mTeg response to ITD can be
515 explained entirely as a linear combination ITD-tuning curves form OT. Therefore, we modeled
516 the responses in mTeg with a weighted sum of the OT population. To estimate the weights of the
517 convergence, we used discrete Fourier transforms (FFT) of the experimental mTeg ITD tuning
518 curves calculated after offsetting the curves to zero mean, as described previously [25]. The
519 weights given by the normalized FFT phase spectra of mTeg neurons were applied to OT
520 neurons with equivalent preferred frequency (Figure 4A,B). The modeled mTeg response was
521 therefore given by: $Y_i(ITD) = \sum_{n=1}^{N} f_{i,n} X_n(ITD)$, where $X_n(ITD)$ is the modeled ITD curve of the
522 n^{th} neuron in OT and $f_{i,n}$ the weights given by the FFT phase spectra of the ith mTeg neurons at
523 the preferred frequency of the nth OT neuron.

524 <u>*Bayesian estimates*</u>*:* A general approach to decoding the neural population activity is to compute
525 a MAP estimate of the environmental property θ using a statistical model of the neural responses
526 [46,55,56]. The MAP estimate of stimulus direction at binaural correlation level *BC* (or stimulus

frequency F) is the value of θ that maximizes the posterior probability, or equivalently the log posterior probability, of θ given the neural activities:

$$\hat{\theta}_{map} = \underset{\theta}{\operatorname{argmax}} \ \ln p(\theta \mid \mathbf{r}, BC) .$$

We computed the MAP estimate of stimulus direction at different BC (or stimulus frequency) values from the model population response assuming Gaussian variability with mean population response $\mathbf{f}(\theta, BC)$ and covariance matrix $\Sigma(\theta, BC)$ and that the determinant of the covariance matrix is constant across stimulus direction. The MAP estimate is computed as:

$$\begin{aligned}\hat{\theta}_{map} &= \underset{\theta}{\operatorname{argmax}} \ \ln p(\theta \mid \mathbf{r}, BC) \\ &= \underset{\theta}{\operatorname{argmax}} \ -\frac{1}{2}(\mathbf{r} - \mathbf{f}(\theta, BC))^T \Sigma^{-1}(\theta, BC)(\mathbf{r} - \mathbf{f}(\theta, BC)) - \frac{|\theta|}{25} .\end{aligned}$$

The covariance matrix $\Sigma(\theta, BC)$ is estimated from the responses of the modeled space-map neurons and takes into account the correlations induced by shared noise at the input. Because we are using a model of the space-map neurons, we can reliably estimate all of the correlations between neurons in the population.

The variability of the MAP estimate for a given stimulus ITD is the standard deviation of the MAP estimate over 50 trials of a stimulus presentation. The overall variability of the MAP estimate as a function of BC was computed as the average standard deviation over all the 21 stimulus ITDs.

ACKNOWLEDGMENTS

This work was funded by NIH grants DC012949 and DC007690. We thank Kourosh Saberi for providing the data used in Fig. 5E and Adam Kohn for comments on the manuscript. Clifford Keller helped hand-raising the owlets and Daniel Munch participated in the blind analysis of behavior.

COMPETING INTERESTS

The authors declare no competing financial interests.

REFERENCES

1 Hausmann, L., von Campenhausen, M., Endler, F., Singheiser, M. & Wagner, H. (2009). Improvements of sound localization abilities by the facial ruff of the barn owl (Tyto alba) as demonstrated by virtual ruff removal. *PloS one* **4**, e7721, doi:10.1371/journal.pone.0007721.

2 Knudsen, E. I., Blasdel, G. G. & Konishi, M. (1979). Mechanisms of sound localization in the barn owl (Tyto alba). *Journal of comparative physiology. A, Sensory, neural, and behavioral physiology* **133**, 13–21.

3 Fischer, B. J. & Pena, J. L. (2011). Owl's behavior and neural representation predicted by Bayesian inference. *Nature neuroscience* **14**, 1061-1066, doi:10.1038/nn.2872.

4 Rich, D., Cazettes, F., Wang, Y., Pena, J. L. & Fischer, B. J. (2015). Neural representation of probabilities for Bayesian inference. *Journal of computational neuroscience* **38**, 315-323, doi:10.1007/s10827-014-0545-1.

5 Girshick, A. R., Landy, M. S. & Simoncelli, E. P. (2011). Cardinal rules: visual orientation perception reflects knowledge of environmental statistics. *Nature neuroscience* **14**, 926-932, doi:10.1038/nn.2831.

6 Schwartz, O., Hsu, A. & Dayan, P. (2007). Space and time in visual context. *Nature reviews. Neuroscience* **8**, 522-535, doi:10.1038/nrn2155.

7 Strutt, J. W. (1907). On our perception of sound direction. *Philos Mag* **13**, 214-232.

8 Blauert, J. *Spatial hearing : the psychophysics of human sound localization*. Rev. edn, (MIT Press, 1997).

9 Knudsen, E. I. & Konishi, M. (1978). A neural map of auditory space in the owl. *Science,New Series* **200**, 795-797.

10 Knudsen, E. I. (1982). Auditory and visual maps of space in the optic tectum of the owl. *The Journal of neuroscience : the official journal of the Society for Neuroscience* **2**, 1177-1194.

11 Cazettes, F., Fischer, B. J. & Pena, J. L. (2014). Spatial cue reliability drives frequency tuning in the Barn Owl's midbrain. *eLife* **3**, doi:10.7554/eLife.04854.

12 Knudsen, E. I. & Knudsen, P. F. (1983). Space-mapped auditory projections from the inferior colliculus to the optic tectum in the barn owl (Tyto alba). *The Journal of comparative neurology* **218**, 187-196, doi:10.1002/cne.902180206.

13 Olsen, J. F., Knudsen, E. I. & Esterly, S. D. (1989). Neural maps of interaural time and intensity differences in the optic tectum of the barn owl. *The Journal of neuroscience : the official journal of the Society for Neuroscience* **9**, 2591-2605.

14 Knudsen, E. I. (1984). Auditory properties of space-tuned units in owl's optic tectum. *Journal of neurophysiology* **52**, 709-723.

15 Masino, T. & Knudsen, E. I. (1992). Anatomical pathways from the optic tectum to the spinal cord subserving orienting movements in the barn owl. *Experimental brain research* **92**, 194-208.

16 Masino, T. & Knudsen, E. I. (1993). Orienting head movements resulting from electrical microstimulation of the brainstem tegmentum in the barn owl. *The Journal of neuroscience : the official journal of the Society for Neuroscience* **13**, 351-370.

17 Masino, T. (1992). Brainstem control of orienting movements: intrinsic coordinate systems and underlying circuitry. *Brain, behavior and evolution* **40**, 98-111.

18 du Lac, S. & Knudsen, E. I. (1990). Neural maps of head movement vector and speed in the optic tectum of the barn owl. *Journal of neurophysiology* **63**, 131-146.

19 Masino, T. & Knudsen, E. I. (1990). Horizontal and vertical components of head movement are controlled by distinct neural circuits in the barn owl. *Nature* **345**, 434-437, doi:10.1038/345434a0.

20 Netser, S., Ohayon, S. & Gutfreund, Y. (2010). Multiple manifestations of microstimulation in the optic tectum: eye movements, pupil dilations, and sensory priming. *Journal of neurophysiology* **104**, 108-118, doi:10.1152/jn.01142.2009.

21 Takahashi, T. & Konishi, M. (1986). Selectivity for interaural time difference in the owl's midbrain. *The Journal of neuroscience : the official journal of the Society for Neuroscience* **6**, 3413–3422.

22 Groh, J. M. (2001). Converting neural signals from place codes to rate codes. *Biological cybernetics* **85**, 159-165.

23 Salinas, E. (2006). How behavioral constraints may determine optimal sensory representations. *PLoS biology* **4**, e387, doi:10.1371/journal.pbio.0040387.

24 Fischer, B. J., Anderson, C. H. & Pena, J. L. (2009). Multiplicative auditory spatial receptive fields created by a hierarchy of population codes. *PloS one* **4**, e8015, doi:10.1371/journal.pone.0008015.

25 Vonderschen, K. & Wagner, H. (2012). Transformation from a pure time delay to a mixed time and phase delay representation in the auditory forebrain pathway. *The Journal of neuroscience : the official journal of the Society for Neuroscience* **32**, 5911-5923, doi:10.1523/JNEUROSCI.5429-11.2012.

26 Saberi, K., Takahashi, Y., Konishi, M., Albeck, Y., Arthur, B.J., Farahbod, H. (1998). Effects of interaural decorrelation on neural and behavioral detection of spatial cues. *Neuron* **21**, 789-798.

27 Cazettes, F., Fischer, B. J. & Pena, J. L. (2016). Cue Reliability Represented in the Shape of Tuning Curves in the Owl's Sound Localization System. *The Journal of neuroscience : the official journal of the Society for Neuroscience* **36**, 2101-2110, doi:10.1523/JNEUROSCI.3753-15.2016.

28 Hazan, Y., Kra, Y., Yarin, I., Wagner, H. & Gutfreund, Y. (2015). Visual-auditory integration for visual search: a behavioral study in barn owls. *Frontiers in integrative neuroscience* **9**, 11, doi:10.3389/fnint.2015.00011.

29 Todorov, E. (2000). Direct cortical control of muscle activation in voluntary arm movements: a model. *Nature neuroscience* **3**, 391-398, doi:10.1038/73964.

30 Overduin, S. A., d'Avella, A., Carmena, J. M. & Bizzi, E. (2012). Microstimulation activates a handful of muscle synergies. *Neuron* **76**, 1071-1077, doi:10.1016/j.neuron.2012.10.018.

31 Joshua, M. & Lisberger, S. G. (2014). A framework for using signal, noise, and variation to determine whether the brain controls movement synergies or single muscles. *Journal of neurophysiology* **111**, 733-745, doi:10.1152/jn.00510.2013.

32 Moiseff, A. (1989). Bi-coordinate sound localization by the barn owl. Journal of comparative physiology A, Sensory, neural, and behavioral physiology 164:637-644

33 Summerfield, C. & de Lange, F. P. (2014). Expectation in perceptual decision making: neural and computational mechanisms. *Nature reviews. Neuroscience* **15**, 745-756, doi:10.1038/nrn3838.

34 Wei, X. X. & Stocker, A. A. (2015). A Bayesian observer model constrained by efficient coding can explain 'anti-Bayesian' percepts. *Nature neuroscience* **18**, 1509-1517, doi:10.1038/nn.4105.

35 Wei, X. & Stocker, A. A. (2012a). Bayesian inference with efficient neural population codes. In Proceedings of the Int'l Conf on Artificial Neural Networks .NewYork:Springer..

36 Jazayeri, M. & Shadlen, M. N. (2010). Temporal context calibrates interval timing. *Nature neuroscience* **13**, 1020-1026, doi:10.1038/nn.2590.

37 Kording, K. P. & Wolpert, D. M. (2004). Bayesian integration in sensorimotor learning. *Nature* **427**, 244-247.

38 Populin, L. C. & Yin, T. C. (1998). Behavioral studies of sound localization in the cat. *The Journal of neuroscience : the official journal of the Society for Neuroscience* **18**, 2147-2160.

39 Nodal, F. R., Bajo, V. M., Parsons, C. H., Schnupp, J. W. & King, A. J. (2008). Sound localization behavior in ferrets: comparison of acoustic orientation and approach-to-target responses. *Neuroscience* **154**, 397-408, doi:10.1016/j.neuroscience.2007.12.022.

40 Zahn, J. R., Abel, L. A. & Dell'Osso, L. F. (1978). Audio-ocular response characteristics. *Sensory processes* **2**, 32-37.

41 Stocker, A. A. & Simoncelli, E. P. (2006). Noise characteristics and prior expectations in human visual speed perception. *Nature neuroscience* **9**, 578-585, doi:10.1038/nn1669.

42 Weiss, Y., Simoncelli, E. P. & Adelson, E. H. (2002). Motion illusions as optimal percepts. *Nature neuroscience* **5**, 598-604, doi:10.1038/nn858.

43 Pouget, A., Dayan, P. & Zemel, R. S. (2003). Inference and computation with population codes. *Annual review of neuroscience* **26**, 381-410, doi:10.1146/annurev.neuro.26.041002.131112.

44 Beck, J. M., Ma, W.J., Kiani, R., Hanks, T., Churchland, A.K., Roitman, J., Shadlen, M.N., Latham, P.E., Pouget, A. (2008). Probabilistic population codes for Bayesian decision making. *Neuron* **60**, 1142-1152, doi:10.1016/j.neuron.2008.09.021.

45 Lochmann, T. & Deneve, S. (2011). Neural processing as causal inference. *Current opinion in neurobiology* **21**, 774-781, doi:10.1016/j.conb.2011.05.018.

46 Ma, W. J., Beck, J. M., Latham, P. E. & Pouget, A. (2006). Bayesian inference with probabilistic population codes. *Nature neuroscience* **9**, 1432-1438, doi:10.1038/nn1790.

47 Wang, Y., Shanbhag, S. J., Fischer, B. J. & Pena, J. L. (2012). Population-wide bias of surround suppression in auditory spatial receptive fields of the owl's midbrain. The Journal of neuroscience : the official journal of the Society for Neuroscience **32**, 10470-10478, doi:10.1523/JNEUROSCI.0047-12.2012.

48 Ter-Mikaelian, M., Sanes, D. H. & Semple, M. N. (2007). Transformation of temporal properties between auditory midbrain and cortex in the awake Mongolian gerbil. The Journal of neuroscience : the official journal of the Society for Neuroscience **27**, 6091-6102, doi:10.1523/JNEUROSCI.4848-06.2007.

49 Schumacher, J. W., Schneider, D. M. & Woolley, S. M. (2011). Anesthetic state modulates excitability but not spectral tuning or neural discrimination in single auditory midbrain neurons. Journal of neurophysiology **106**, 500-514, doi:10.1152

50 Knudsen, E. I., konishi, M. & Blasdel, G. G. (1979). Sound Localization by the Barn Owl (Tyto alba) Measured with the Search Coil Technique. J. Comp. Physiol. **133**, 1-11.

51 Ohayon, S., van der Willigen, R. F., Wagner, H., Katsman, I. & Rivlin, E. (2006). On the barn owl's visual pre-attack behavior: I. Structure of head movements and motion patterns. Journal of comparative physiology. A, Neuroethology, sensory, neural, and behavioral physiology **192**, 927-940, doi:10.1007/s00359-006-0130-9.

52 Koppl, C. (1997). Frequency tuning and spontaneous activity in the auditory nerve and cochlear nucleus magnocellularis of the barn owl Tyto alba. Journal of neurophysiology **77**, 364-377.

53 Mysore, S. P. & Knudsen, E. I. (2012). Reciprocal inhibition of inhibition: a circuit motif for flexible categorization in stimulus selection. Neuron **73**, 193-205, doi:10.1016/j.neuron.2011.10.037.

54 Mysore, S. P. & Knudsen, E. I. (2014). Descending control of neural bias and selectivity in a spatial attention network: rules and mechanisms. Neuron **84**, 214-226, doi:10.1016/j.neuron.2014.08.019.

55 Salinas, E. & Abbott, L. F. (1995). Transfer of coded information from sensory to motor networks. The Journal of neuroscience : the official journal of the Society for Neuroscience **15**, 6461-6474.

56 Seung, H. S. & Sompolinsky, H. (1993). Simple models for reading neuronal population codes. Proceedings of the National Academy of Sciences of the United States of America **90**, 10749-10753.

707 **FIGURES & FIGURE LEGENDS**

708

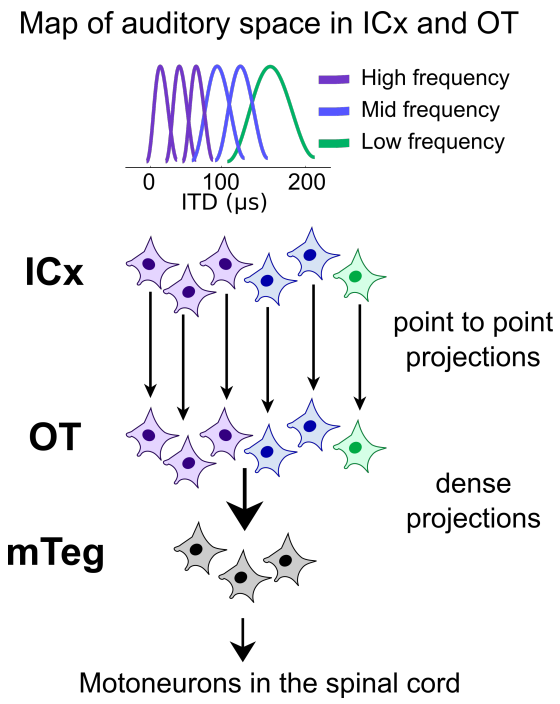

709

710 **Figure 1.** Sound localization pathway. ICx and OT display maps of frequency and space. Frontal

711 space (small ITD in µs in purple) is associated with high frequency. Conversely, peripheral space

712 (large ITD in µs in green) is associated with low frequency. Although OT directly projects to

713 mTeg, the nature of the projection between OT and mTeg is unknown.

714

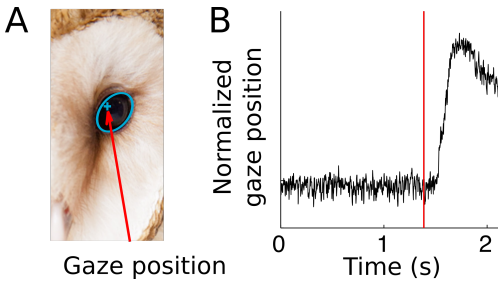

Figure 2. Microstimulation in mTeg elicits eye movements. (A) An eye tracking system detected the pupil (blue ellipse) and the position of the corneal reflection (blue cross) over time. (B) Microstimulation (red line) through the recording electrode elicited eye movements detected by the eye tracker.

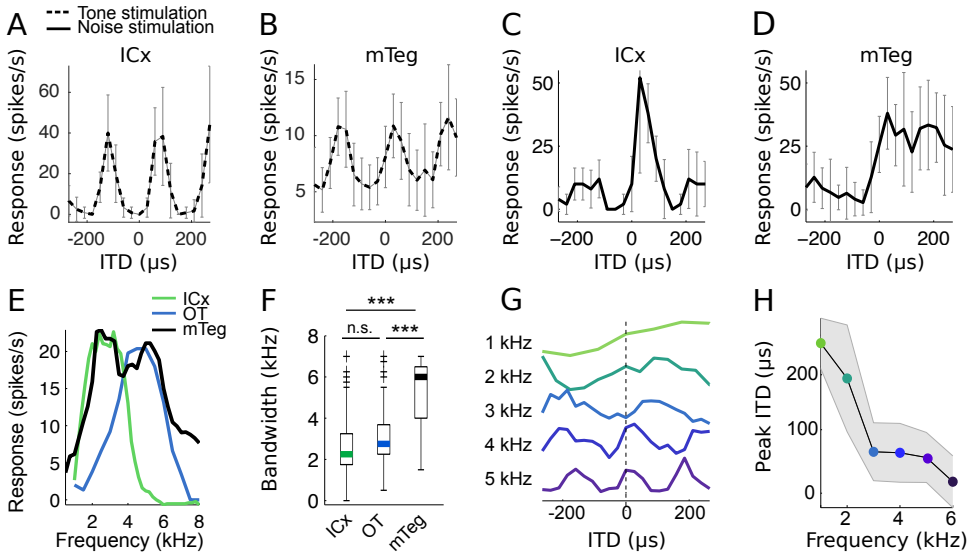

Figure 3. Tuning properties in the space-map and mTeg. (A,B) Example ITD tuning curves (mean and standard deviation across trials) of ICx (A) and mTeg (B) neurons for tonal stimulation. (C,D) Example ITD tuning curves (mean and standard deviation across trials) of ICx (C) and mTeg (D) neurons for broadband noise. (E) Example frequency tuning curve of an mTeg neuron (black) superimposed with frequency tuning curves of ICx (green) and OT (blue) cells showing the broader frequency tuning in mTeg. (F) Across the samples, mTeg neurons (n=36 from Owls #1, 2 & 3) were significantly more broadly tuned than ICx (n=184 from Owls #1, 2 & 3) and OT (n=39 from Owls #4, 5 & 6) cells (***$p<0.001$). (G) Example ITD tuning curves of an mTeg neuron for different frequencies, showing that ITD tuning varied with frequency. (H) The mean and standard deviation of peak ITDs for tonal stimulation across the mTeg sample. The mean peak ITD varied with stimulus frequency.

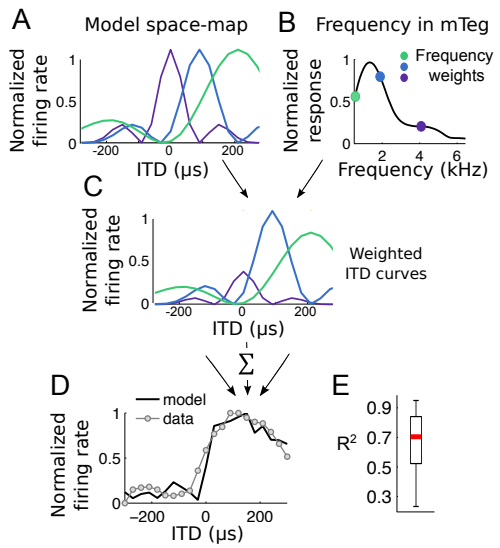

Figure 4. Convergence from the space-map into mTeg. (A) Model of frequency-dependent ITD tuning curves in the space map. Neurons tuned to small ITDs preferred high frequencies (purple), neurons tuned to intermediate ITDs preferred intermediate frequencies (blue) and neurons tuned to larger ITDs preferred low frequencies (green). (B) The weights for each frequency (normalized from 0 to 1) were estimated from the Fourier decomposition of responses of mTeg neurons to broadband sound, on a neuron-by-neuron basis. (C) Space-map ITD tuning curves (A) scaled by the weights estimated in (B) and summed to simulate the convergence. (D) Example experimental ITD-tuning curve in mTeg (gray dotted line) and the output of the convergence model with the respective weights. (E) The boxplot shows the median and quartiles of the coefficient of determination (r^2) between modeled and measured mTeg ITD curves across the sample.

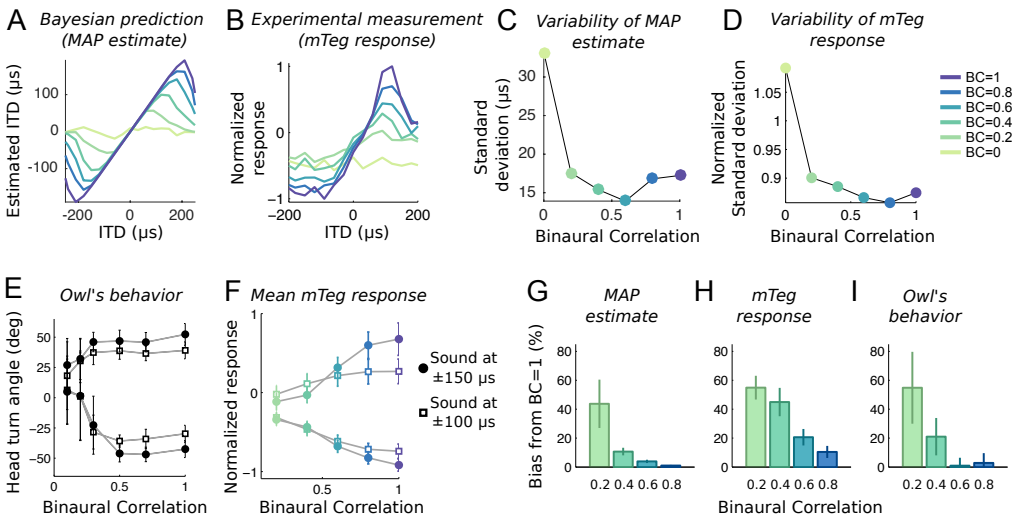

Figure 5. The owl's behavioral bias under varying levels of noise is predicted by the MAP estimate and mTeg responses. (A) MAP estimate with varying BC (high to low BC indicated by changing from blue to green). (B) Mean ITD-response in mTeg for varying BC. To calculate the mean ITD-response in mTeg, the ITD-response of each neuron was first normalized to its mean activity at BC=1 before taking the average of the ITD-response across all the recorded neurons. (C) Mean standard deviation over 15 ITDs and 50 iterations of the MAP estimate. (D) Mean over 21 ITDs of the standard deviation of the mean mTeg response. (E) Mean and standard deviation of the owl's head orienting response as a function of BC (modified from [26]). Behavioral responses to four different ITDs are shown (actual values indicated on the right). The centrality bias increases as BC decreases. (F) Mean mTeg response across BC for similar ITDs as in (E). (G,H,I) Reduction in response from the BC = 1 condition, which quantify the bias toward the center, computed as the mean difference between responses at BC=1 and other BCs at the same four directions shown in (E) and (F). Error bars in (F) and (G,H,I) represent s.e.m.

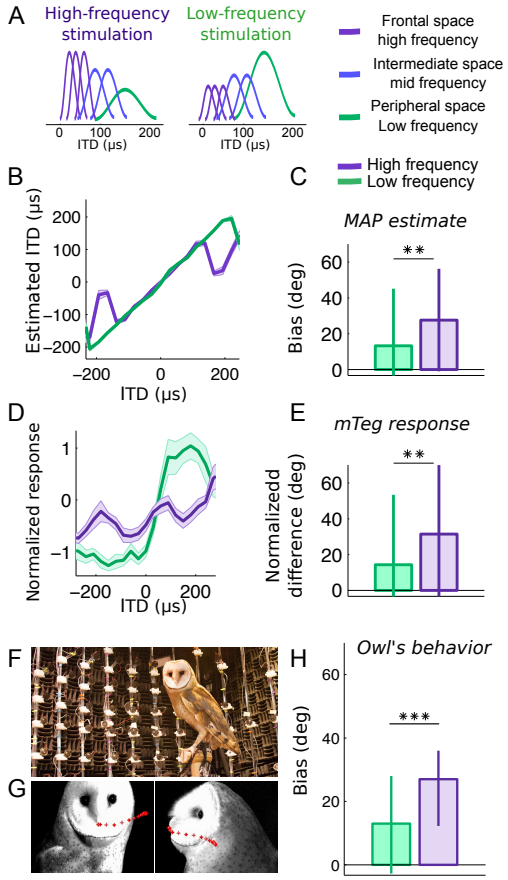

Figure 6. Changes in the owl's behavioral bias induced by manipulating stimulus frequency. (A) Schematic population of space-map neurons whose relative response rate varies with the frequency of the stimulating sound. Stimulation with high frequencies (middle) excites more strongly the frontal neurons, which prefer higher frequencies. Conversely, stimulation with low frequencies (bottom) excites more strongly the peripheral neurons. (B) MAP estimate for sound stimulation of varying frequency as described in (A) (shaded areas are s.e.m). (C) Mean and standard deviation over sound directions (ITD > 50 μs and ITD < -50 μs) of the bias predicted by MAP estimate (in B). (D) Mean ITD tuning across mTeg neurons for varying frequency. (E) Mean and standard deviation of the difference in bias between stimulating conditions predicted

from the mTeg responses across ITD. To compute the relative change in bias predicted by the mTeg responses at high and low frequency, we measured the amplitude difference between the two curves. To compare the biases predicted by the mTeg responses and MAP estimate, we used the MAP estimate at low frequency as common scale for both datasets. Therefore, the mTeg responses were normalized so that the maximum value of the mTeg response at low frequency matches the maximum of the MAP estimate at low frequency. (F) Owls were trained to stand on a perch at the center of a speaker array. (G) Images captured by two high-speed infrared video cameras at different angles. The owl's head was tracked as it moved in space. Red dotted lines indicate the trajectory preceding the shown images. (H) Median and quartiles of the bias of head-orienting responses from three barn owls presented with high-frequency (n=47) and low-frequency (n=36) bandpass noise. (c,e,h) *$p<0.05$, **$p<0.01$, ***$p<0.001$, high frequency in purple and low frequency in green.

SUPPLEMENTARY FIGURES

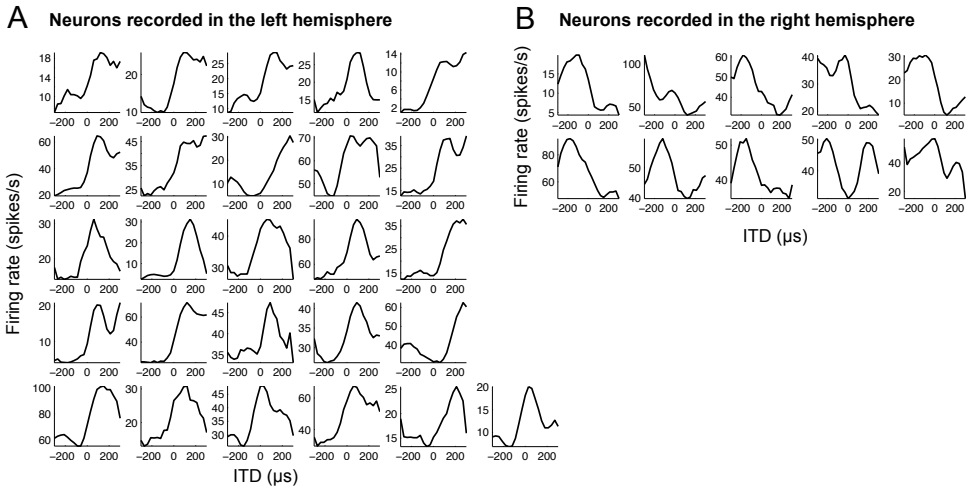

Supplementary Figure S1. ITD tuning from broadband noise stimulation of 36 mTeg neurons recorded in 3 barn owls (1 male and 2 females). (a) Neurons in the left hemisphere display a peak or a plateau of activity at positive ITDs. (b) Neurons in the right hemisphere display a peak or a plateau of activity at negative ITDs. Overall, neurons respond maximally to the contralateral side.

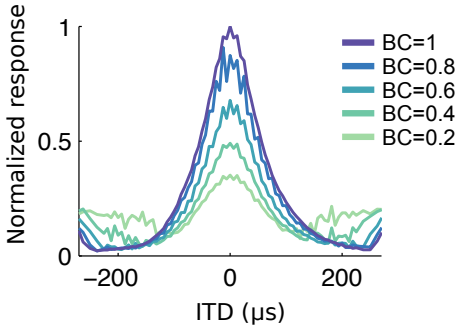

Supplementary Figure S2. Mean modeled response of a random linear convergence from the space-map onto mTeg at different values of binaural correlation (BC). The convergence was modeled using the method described in the manuscript, except that weights were random (sampled uniformly from 0 to 1) rather than estimated from the Fourier transform of mTeg ITD curves. The random linear convergence does not predict the mTeg response, nor approximate a Bayesian decoder.

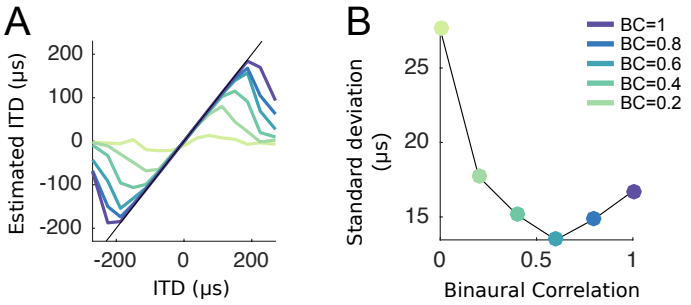

Supplementary Figure S3. Posterior mean estimate at different values of binaural correlation (BC) (a) Posterior mean estimate with varying BC (high to low BC indicated by changing from blue to green). (b) Mean over 15 ITDs of the standard deviation over 50 trials of the posterior mean estimate.

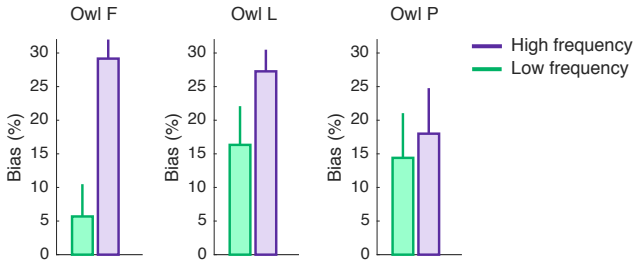

Supplementary Figure S4. Mean and s.e.m of the bias of head-orienting responses from three barn owls (F, L and P) presented with high-frequency and low-frequency bandpass noise.